# Special Pair Dance and Partner Selection: Elementary Steps in Proton Transport in Liquid Water

**Omer Markovitch,[‡,#] Hanning Chen,[†] Sergei Izvekov,[†] Francesco Paesani,[†] Gregory A. Voth,[†] and Noam Agmon*[,‡]**

*Institute of Chemistry and the Fritz Haber Research Center, The Hebrew University of Jerusalem, Jerusalem 91904, Israel, and the Department of Chemistry and the Henry Eyring Center for Theoretical Chemistry, University of Utah, Salt Lake City, Utah 84112-0850*

*Received: May 07, 2008*

Conditional and time-dependent radial distribution functions reveal the details of the water structure surrounding the hydronium during the proton mobility process. Using this methodology for classical multistate empirical valence bond (MS-EVB) and ab initio molecular dynamics trajectories, as well as quantal MS-EVB trajectories, we supply statistical proof that proton hops in liquid water occur by a transition from the $H_3O^+[3H_2O]$ Eigen-complex, via the $H_5O_2^+$ Zundel-complex, to a $H_3O^+[3H_2O]$ centered on a neighboring water molecule. In the "resting period" before a transition, there is a distorted hydronium with one of its water ligands at a shorter distance and another at a longer distance than average. The identity of this "special partner" interchanges rapidly within the three first-shell water ligands. This is coupled to cleavage of an acceptor-type hydrogen bond. Just before the transition, a partner is selected by an additional translation of the $H_3O^+$ moiety in its direction, possibly enabled by loosening of donor-type hydrogen bonds on the opposite side. We monitor the transition in real time, showing how the average structure is converted to a distorted $H_5O_2^+$ cation constituting the transitional complex for proton hopping between water molecules.

## Introduction

Protons participate in numerous chemical reactions, from acid−base solution-phase reactions to enzymatic catalysis. It is pivotal in corrosion processes, atmospheric chemistry, energy transduction in the living cell, and the construction of hydrogen fuel cells.[1–6] Its mobility in liquid water is at least 4.5 times larger than that of any other cation. Elucidating the details of this unusual phenomenon is fundamental for the understanding of the numerous processes in which protons participate.

200 years ago, Grotthuss has suggested a chain mechanism for shuttling hydrogen atoms in the electrolysis of water (depicted then as OH).[7,8] When ions and protons were discovered, the Grotthuss mechanism was revived as a mechanism for proton mobility,[9–11] which is transferred from one water molecule to its neighbor without requiring extensive translation of the oxygen atoms. This explained its fast mobility. Yet the molecular mechanism behind this shuttling process remained an enigma.

Hückel postulated that $H_3O^+$ rotation is the basis for proton transfer (PT) in liquid water.[12] Bernal and Fowler perceived the proton as hopping from $H_3O^+$ onto a nearby rotating water molecule once it achieves the correct orientation.[13] Eigen suggested fast PT along a hydrogen-bonded chain of water molecules.[14] Finally, PT was proposed to consist of isomerization between two protonated water conformations:[15–18] the more stable $H_3O^+[3H_2O]$ complex ("the Eigen cation")[14] and the transition structure $H_5O_2^+$ ("the Zundel cation");[11,19] see Figure 1. We term this the "Eigen−Zundel−Eigen" (EZE) transition.

By that time molecular dynamics (MD) methodologies for simulating proton in water came of age.[20–38] Using the ab initio molecular dynamics (AIMD) methods of Car and Parrinello,[39] Tuckerman et al. simulated a proton with 32 water molecules for 4 ps.[20,21] They observed "special-pair" formation between $H_3O^+$ and one of the three water molecules in its first solvation shell, which was under-coordinated and at a shorter distance than the other two. The identity of the special partner switched with time, representing either fluctuations in a distorted Eigen complex,[32] or a Zundel (through Eigen) to Zundel (ZZ) transition (cf. Figure 1 in ref 5). Thus, the precise interpretation of the pioneering AIMD studies[20,21] awaited clarification.

Using different multistate generalizations of a two-state empirical valence bond (EVB) model[40] for proton hopping between water molecules,[24] Voth and co-workers[31–36] and Vuilleumier and Borgis[27–30] analyzed the PT mechanism in liquid water. Vuilleumier and Borgis reported that PT involved a ZZ transition,[30] while Voth and co-workers found evidence supporting an EZE mechanism,[31–37] with the Eigen cation more stable than the Zundel cation by 3.5 kJ/mol.[37] This result is in agreement with an earlier qualitative estimate based on correlating hydrogen-bond (HB) lengths with HB energies.[17] Other theoretical methods also yielded conflicting results: The EZE scenario found strong support in ab initio path integral study,[23] although introduction of quantum effects makes the energetic difference between Eigen and Zundel cations smaller than in the classical limit.[41] In contrast, a recent calculation utilizing "quasi-chemical theory" found that the Zundel cation is more stable than the Eigen cation by about 33 kJ/mol.[42] Other studies suggested that second-neighbor jumps are rate limiting.[43]

Recent experimental data from acidified liquid water helped elucidating the nature of the Grotthuss mechanism. Time-resolved IR[44,45] detected the transient relaxation of the Eigen cation. Photoelectron spectroscopy[46,47] demonstrated that the

* Corresponding author. E-mail: agmon@fh.huji.ac.il.
‡ The Hebrew University.
† University of Utah.
# Current address: Department of Structural Biology, Weizmann Institute of Science, Rehovot 76100, Israel.

10.1021/jp804018y CCC: $40.75 
Published on Web 07/16/2008

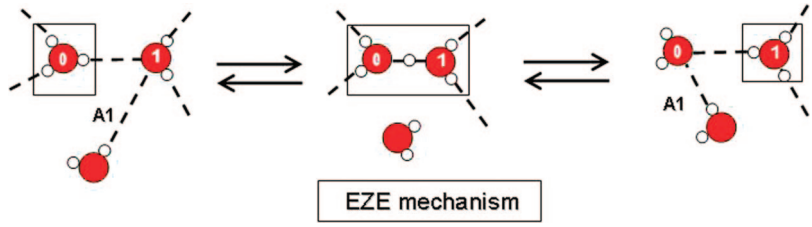


**Figure 1.** Eigen−Zundel−Eigen (EZE) proton mobility mechanism of refs 15 and 16. Oxygens in red. HBs are depicted by dashed lines. See Figure S1 in ref 48 for a comparison with the ZZ mechanism.

Eigen cation is indeed more stable than the Zundel cation, so that protons migrate in liquid water by the EZE mechanism,[46,47] as suggested by theory.[15–18,23,31–37] Here, we introduce conditional and time-dependent radial distribution function (RDF) for identifying the Eigen and Zundel cations, and validating the EZE mechanism statistically for a wide-range of simulation methodologies.

While literature converges on the EZE scenario, its coupling to the HB dynamics of liquid water remains enigmatic. Cleavage of HB accepted by a first-shell water ligand of the hydronium was suggested to constitute the rate-limiting step for PT.[15,16,20,21] This was questioned by a series of subsequent MD studies,[30,34,36,48] prompting us to revisit the question of proton mobility in more detail than before.

Clearly, a mechanism is never a realization of a single trajectory[49] but represents in some sense a statistical average over an ensemble of trajectories. Thus, finding suitable statistical measures is one aspect of the present work. Additionally, one worries whether certain features of the mechanism are unique to a particular simulation model. To address this, we have carried out the current study on a wide array of protonated water models. These include classical multistate-EVB (MS-EVB)[31,32] and AIMD trajectories,[39,50,51] as well as a quantal MS-EVB trajectory using centroid molecular dynamics (CMD),[52] all showing qualitatively consistent behavior. We find that PT in liquid water is actually not a single-step process. Rather, it occurs hierarchically,[36] on multiple time and distance scales. First, there is a period during which the hydronium exchanges its closest partner without actual PT occurrence. This "special-pair dance" (SP-dance) terminates when a final partner for PT is selected. Only then a proton hop occurs. Failure to realize the multistep nature of PT in water may have contributed to some of the above-mentioned confusion in the literature.

## Methods

We have run five different types of trajectories for a (single) proton in a box of $N$ water molecules (total of $3N + 1$ nuclei) at 300 K. Four were classical trajectories, and one was quantal. Two types of potentials for aqueous proton were utilized: (a) MS-EVB potentials of (i) second generation (MS-EVB2)[35] and (ii) third generation (MS-EVB3).[37] These potentials are based on a water force-field augmented by the adiabatic valence-bond states of a proton attached to different water molecules. They have been calibrated against high-level ab initio and experimental data, allowing efficient generation of protonated water trajectories.[35,37] The second type of potential is (b) AIMD based on "on the fly" potentials,[39] generated using density functional theory (DFT) with two types of functionals: (i) the traditional BLYP functional and (ii) the HCTH/120 functional,[53] recently advocated as more reliable for the simulation of both water[51] and protonated water,[50] when employing a plane-wave basis set and other widely used conditions for CPMD simulations. In addition to the four classical simulations for the MS-EVB2, MS-EVB3, BLYP, and HCTH models, we have generated quantal trajectories for the MS-EVB3 potential (qMS-EVB3) using CMD.[52] Results for the less up-to-date potentials, MS-EVB2 and BLYP, are delegated to the Supporting Information.

The run-time parameters for our trajectories are summarized in Table 1. For MS-EVB2 and MS-EVB3, it is possible to generate very long trajectories (large $t_{max}$), but the other methodologies are more costly hence these trajectories are considerably shorter, leading to more pronounced noise in our statistical analysis below but without affecting the qualitative conclusions.

**TABLE 1: Parameters Characterizing the Different Trajectories Run in This Work**

| method | $\Delta t$,[a] fs | $N$[b] | $l_{box}$,[c] Å | $t_{max}$,[d] ps | $\Delta t$,[e] fs |
|---|---|---|---|---|---|
| HCTH | 0.073 | 64 | 12.43 | 96 | 3.63 |
| MS-EVB3 | 0.5 | 216 | 18.62 | 6000 | 5 |
| qMS-EVB3 | 0.01 | 216 | 18.62 | 1060 | 5 |
| MS-EVB2 | 0.5 | 216 | 18.64 | 2000 | 5 |
| BLYP | 0.073 | 64 | 12.43 | 30 | 3.63 |

[a] Propagation time-step. [b] Number of water molecules in simulation box. [c] Length of simulation box. [d] Overall trajectory time-length. [e] Time-interval for saving the coordinates.

For the MS-EVB3 model,[37] three independent trajectories were run. For each trajectory, after 1 ns equilibration in the NVT ensemble with a target temperature of 300 K, a production run of 2 ns was performed in the NVE ensemble. The dynamical quantities were thus obtained by averaging over a total of 6 ns of NVE simulations. A more specific and detailed description of the MS-EVB3 method is reported in ref 37.

For the AIMD trajectories, the simulated system consisted of 64 water molecules and one excess proton. A standard implementation of the Car−Parrinello molecular dynamics (CPMD) method was adopted,[39] using a plane-wave-basis DFT with a cutoff of 80 Ry. Version 3.11 of the publicly available code was used.[54] The ion−electron interaction was described by Troullier−Martins type pseudopotentials,[55] while the HCTH/120 or BLYP exchange correlation functional was employed to describe the electronic interactions.[53] The hydrogen nucleus was assigned a protonic mass. We used a fictitious electronic mass $\mu$ of 340 au, that is consistent with the convergence criterion of Schwegler et al.[56] for CPMD simulations of hydrogen-containing systems. Higher values of $\mu$ may result in artifacts in structural and dynamic properties of liquid water.[57]

Given the high computational cost of a CPMD simulation, the pure water system was pre-equilibrated for 50 ps in an empirical MD simulation using a force field developed from a force-matching of the HCTH/120 or BLYP CPMD simulation of liquid water. After an excess proton was added to the resulting configuration, the system was additionally equilibrated for 4 ps using CPMD with simple velocity rescaling to maintain a target

ionic temperature of 300 K. A production run was then performed in the constant NVE ensemble for the duration given in Table 1. The average temperature in the CPMD simulation was $T = 298.6$ K. In Supporting Information, we utilize the BLYP CPMD trajectory from ref 50.

For the qMS-EVB3 method, CMD simulations were performed in the NVE ensemble with the centroid force computed on-the-fly according to the adiabatic time scale separation scheme.[52] After an equilibration of 500 ps, the final quantum results were calculated by averaging over 9 independent trajectories of ~100 ps each. A more comprehensive description of the qMS-EVB3 model can be found in ref 37.

In analyzing trajectory results, we first define the hydronium (i.e., the $H_3O^+$ complex) from a geometric criterion as the oxygen with the three closest hydrogen atoms. Its oxygen is perceived as the center of the complex and, accordingly, denoted by $O_0$. The three oxygen atoms in the first solvation-shell are divided into the closest oxygen (denoted by $O_{1x}$) and the two which are further away (denoted jointly by $O_{1yz}$, or according to their increasing distance from the hydronium by $O_{1y}$ and $O_{1z}$, respectively). This arrangement is depicted in Figure 2. We focus below on the dynamics of these four oxygens. To underline new observables considered herein for the first time, we depict them in color, restricting black drawings to data types that have been previously reported in the literature.

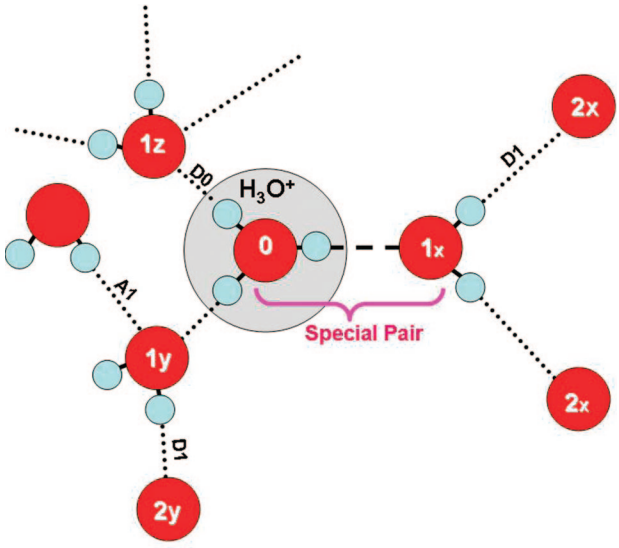


**Figure 2.** Water cluster surrounding the hydronium, $H_3O^+$, in liquid water. First- and second-shell water ligands are denoted by the indices 1 and 2; donor and acceptor HBs are denoted by D and A, respectively. The closest water ligand in the first-shell is denoted by $x$ whereas the other two water molecules are denoted by $y$ and $z$. This notation carries over to the second-shell as well.

## Results and Discussion

**Non Transfer Intervals.** The main goal of the present work is to characterize the behavior of the hydrated proton in the periods between PT events. First, let us consider how these events appear in a typical simulation. Each atom is assigned a fixed number throughout the simulation (its "identity"), so we can monitor the identity of $O_0$, $O_{1x}$, $O_{1y}$, and $O_{1z}$ as a function of time. Figure 3 shows how the identity of the first two varies during a short trajectory segment of 3 ps (HCTH, MS-EVB3, and qMS-EVB3 models). This short segment is chosen for visibility, but the behavior shown is typical of any short segment from the same trajectory. Additional examples (BLYP, MS-EVB2) are given in Figure S1 of Supporting Information. Usually only the identity of the hydronium oxygen is presented in the literature, and this is augmented here by showing the identity of its $1x$ partner (the oxygen atom closest to the hydronium).

PT events appear as abrupt identity changes for $O_0$ (Figure 3, bottom panels). Most of these are nonproductive PTs which promptly reverse their direction. Only a few are successful, leading to a lasting PT. In fact, during the 3 ps trajectory segments shown, there is hardly any successful PT event. Unlike a previous work from our groups which focused only on successful events,[36] we do not differentiate here between the two kinds.

The PT events divide the time axis into segments ("non-transfer intervals"). At the beginning of each segment, a new hydronium is formed, and it is maintained continuously until the end of the segment, when the proton moves to another oxygen. Figure 4 shows the fraction of segments which are longer than $t$ as a function of time. This is the same as the probability that the proton has not transferred until time $t$,[58] which is known as the "history dependent"[59,60] or "continuous" correlation-function, $C(t)$. It decays multiexponentially:[35] The two longer exponents are similar to those found by Chandra et al.[58] and attributed by them to "proton rattling" (recurrent PT events). We find a third, short time-constant of about 6 fs, likely due to "ballistic" motion of the central proton within a tight Zundel complex. Analysis of such correlation functions provides information on the timescales of dynamic processes but not on the participating molecular structures. The present work focuses on structural changes that occur within the non-transfer intervals.

These intervals are classified as "Short" and "Long" when the structure of the hydrated proton approaches that which is observed for infinitely short or infinitely long intervals, respectively. The flickering events tend to cluster, creating an abundance of short intervals. During these intervals, $O_0$ and $O_{1x}$ interchange their identities rapidly. The complementary behavior then observed in the two panels of Figure 3 reflects fluctuations between the same two values. In addition, the trajectory exhibits long "resting periods" when no PT takes place and the identity of $O_0$ remains constant. During these "Long" segments, the $O_{1x}$ atom changes its identity between three values. We shall elaborate on this effect below.

For the quantal trajectory (qMS-EVB3, Figure 3) and for the classical MS-EVB2 trajectory (Figure S1), the PT frequency is considerably higher, commensurate with the larger proton mobility calculated for these systems.[37] Hence, there are fewer long segments in these cases. For example, the fraction of segments longer than 500 fs is 0.001 for qMS-EVB3, as compared with 0.004 for MS-EVB3 and AIMD/HCTH.

From the above discussion, it is reasonable to expect that during the long segments the hydronium has one structure, typical of its resting state, whereas during the short segments it is characterized by another structure, possibly the transition-state structure for PT in liquid water. We utilize this idea in analyzing equilibrium, conditional and time-dependent RDFs which characterize the various structures of protonated water that participate in the proton mobility process.

**Equilibrium RDFs and the Special Pair.** The radial distribution function, $g(r)$, is a fundamental property of liquid structure.[61] Centered on a fixed atom, it measures the number of atoms of a given type whose center falls at distances between $r$ and $r + dr$ from the fixed atom. For a perfect crystal, it is an oscillating function whose $j$th peak corresponds to the $j$th nearest neighbor. In liquids, the structure fades away after just a few

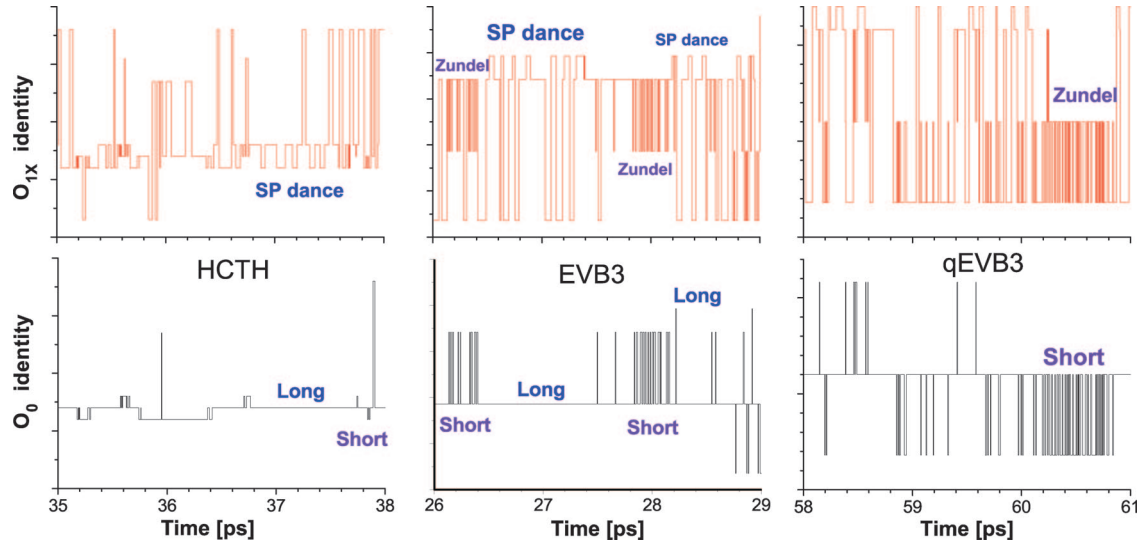


**Figure 3.** Time-dependence of the identity of the hydronium oxygen atom, $O_0$ (bottom, black), and its nearest neighbor oxygen, $O_{1x}$ (top, red), from HCTH, MS-EVB3, and qMS-EVB3 trajectory segments. Longer data for the $O_0$ identity from the HCTH trajectory is shown in Figure 5c of ref 50. See Figure S1 in Supporting Information for similar results for the other simulation models.

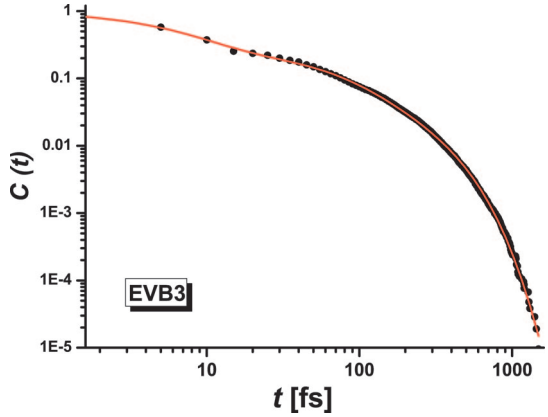


**Figure 4.** Statistics of the "non-transfer intervals" is identical to the correlation function, $C(t)$, which measures the probability of the proton to reside continuously on a single oxygen atom until time $t$. The triple exponential decay (line) fitted to data from the MS-EVB3 trajectory (symbols) has time constants of 6, 54, and 173 fs, with amplitudes of 0.71, 0.21, and 0.08, respectively.

layers and $g(r) \rightarrow 1$ over sufficiently large distances for which only the average density, $\rho_0$, is discernible. With this normalization, the spatial integral of $g(r)$ gives the number of neighbors, $n$, between the specified integration limits ($r_1$ and $r_2$):

$$n = 4\pi\rho_0 \int_{r_1}^{r_2} g(r) r^2 dr \qquad (1)$$

The $r_i$ are typically taken at consecutive minima of $g(r)$, and then $n$ is the average coordination number for the relevant solvation shell.

In the literature, one usually displays only $g_0(r)$,[32,50,62] which is reproduced (for the MS-EVB3 potential) in Figure 5. It has a single peak around 2.5 Å whose area corresponds to a coordination number of about 3 (Table 2). One might think that this peak arises from three equivalent bonds in the first-shell of the $H_3O^+$, but this is not so. Pratt and co-workers[42] decomposed it into three peaks corresponding to its three ordered first-shell neighbors (broken lines in the figure). The upper panel shows the indefinite integral of these peaks which, by definition, reach the ultimate value of 1. Their midpoints are at 2.43, 2.53, and 2.63 Å. The fact that one water molecule (1$x$ in our notation) is closer to the hydronium than the others was first reported by Tuckerman et al.,[21] who termed the 0−1$x$ partners "the special pair". This has led to an assertion that what is observed is a distorted Zundel cation.[5,42] We show below that the structure of the solvated proton is best described as a distorted Eigen cation.[32]

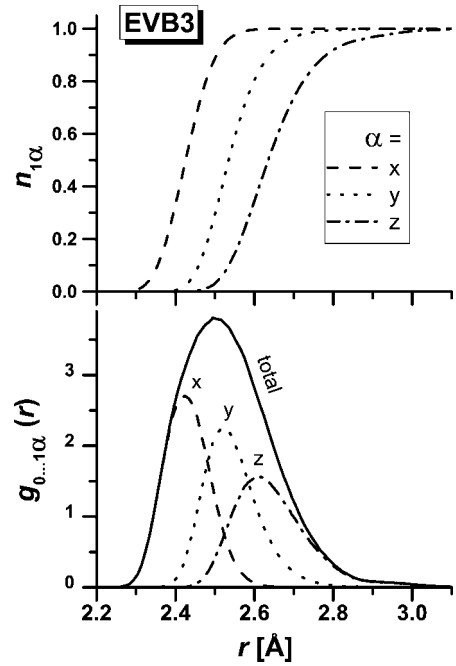


**Figure 5.** (A) Partial RDFs for the three closest neighbors of the hydronium. Symbols: $x$, closest neighbor; $y$, intermediate; $z$, furthest neighbor. Full line (denoted "total") represents their averaged RDF, $g_0(r)$. (B) The corresponding indefinite integrals, eq 1.

To verify this, we consider also the RDFs centered on the first-shell oxygen atoms (see notation in Figure 2). Figure 6 shows the RDFs for (a) the hydronium, $g_0(r)$, (b) its closest nearest neighbor, $g_{1x}(r)$, and (c) the two other water ligands in the first solvation shell, $g_{1yz}(r)$. These were averaged over the whole ensemble of trajectory time-frames, for three types of

**TABLE 2: Coordination Numbers for the First-Shell Neighbors of $O_0$ from $g_0(r)$ of the Equilibrium (Equil.) and Conditional Ensembles (Long and Short Trajectory Segments) of Figures 6 and 9, Respectively[a]**

| method | $r_1$ | $r_2$ | $n$ (Equil.)[b] | $n$ (Long)[b] | $n_1$ (Short)[c] | $n_2$ (Short)[d] |
|---|---|---|---|---|---|---|
| HCTH | 2.52 | 3.05 | 3.0 | 3.1 | 1.3 | 1.9 |
| MS-EVB3 | 2.45 | 2.90 | 3.1 | 3.1 | 1.1 | 1.9 |
| qMS-EVB3 | 2.48 | 2.95 | 2.8 | 2.3 | 1.0 | 1.7 |
| MS-EVB2 | 2.45 | 2.95 | 3.0 | 3.0 | 1.1 | 1.8 |
| BLYP | 2.53 | 3.00 | 3.2 | 3.1 | 1.2 | 2.1 |

[a] $n$ was calculated using eq 1 with the listed integration limits (in Å). These were taken at the minimum of each RDF, with similar values picked for each potential. For the short segments $n = n_1 + n_2$, where $n_1$ and $n_2$ correspond to the two peaks in $g_{1x}(r)$. [b] Integrated from 0 to $r_2$. [c] Integrated from 0 to $r_1$. [d] Integrated from $r_1$ to $r_2$.

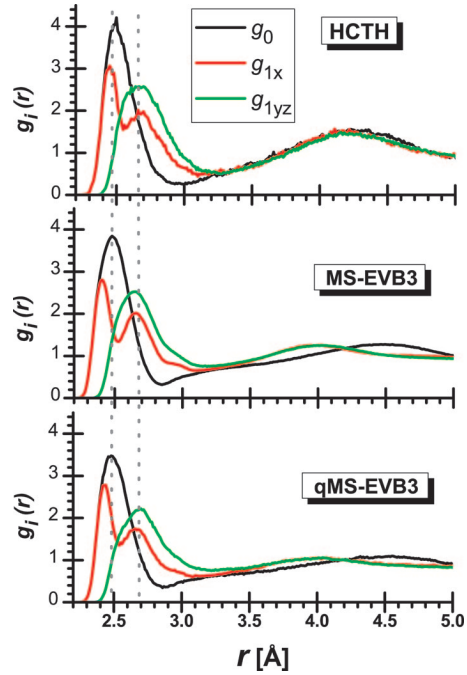


**Figure 6.** Three radial distribution functions as calculated from the complete time-sequence ("equilibrium ensemble") of several simulation algorithms: black, $g_0(r)$; red, $g_{1x}(r)$; green, $g_{1yz}(r)$. Peak locations are marked by the dotted lines. The corresponding coordination numbers are collected in Table 2. See Figure S2 in Supporting Information for similar results for the other simulation models. See also Figure 2 in ref 48.

trajectories (HCTH, MS-EVB3, qMS-EVB3). Additional examples (BLYP, MS-EVB2) are given in Figure S2 of Supporting Information.

Had $O_0$ and $O_{1x}$ been equal partners within a Zundel cation, $g_0(r)$ and $g_{1x}(r)$ would have been approximately equivalent. However, the figure shows that they are drastically different. $g_0(r)$ has a single broad peak which can be decomposed as in Figure 5 above. In contrast, $g_{1x}(r)$ has two peaks for its first-shell neighbors: One around 2.42 Å ($n_1 \approx 1$ in Table 3) is due to the HB with $O_0$, and another near 2.65 Å to HBs with $O_{2x}$ in the second layer ($n_2 \approx 2$). The latter nearly coincides with the peak of $g_{1yz}(r)$.

It follows that the hydronium structure is, on average, a nonsymmetric Eigen cation centered on $O_0$ and forming one short HB in a "special pair" (SP) with $O_{1x}$.[21] This distortion is only part-way in the direction of a Zundel dimer,[32] but this suffices for $O_{1x}$ to have a reduced coordination number of $n = n_1 + n_2 = 3.1$, as compared with 3.7 for $O_{1yz}$ (MS-EVB3, Table 3). We interpret this as a missing A1 bond to $O_{1x}$ (Figure 2), which is by far the weakest HB within the first-shell.[48] The distorted symmetry appears to stabilize the hydronium, perhaps by a pseudo-Jahn−Teller effect.

**TABLE 3: Nearest-Neighbor Numbers for the First-Shell Neighbors of $O_{1x}$ from $g_{1x}(r)$ of the Equilibrium (Equil.) and Conditional Ensembles (Long and Short Trajectory Segments) of Figures 6 and 9, Respectively[a]**

| method | $O_{1x}$: Equilibrium | | | | Long | | | Short | | | $O_{1yz}$: equil. | |
|---|---|---|---|---|---|---|---|---|---|---|---|---|
| | $r_2$ | $r_1$ | $n_1$ | $n_2$ | $r_1$ | $n_1$ | $n_2$ | $r_1$ | $n_1$ | $n_2$ | $r$ | $n$ |
| HCTH | 3.05 | 2.52 | 1.0 | 2.1 | 2.56 | 1.1 | 2.2 | 2.52 | 1.4 | 1.8 | 3.2 | 3.54 |
| MS-EVB3 | 3.00 | 2.55 | 1.2 | 1.9 | 2.55 | 1.1 | 2.0 | 2.45 | 1.1 | 2.1 | 3.2 | 3.72 |
| qMS-EVB3 | 3.00 | 2.55 | 1.1 | 1.7 | 2.55 | 0.83 | 1.8 | 2.48 | 1.1 | 1.6 | 3.2 | 3.40 |
| MS-EVB2 | 2.95 | 2.55 | 1.2 | 1.6 | 2.55 | 1.1 | 1.6 | 2.45 | 1.1 | 1.9 | 3.2 | 3.58 |
| BLYP | 3.10 | 2.53 | 1.0 | 2.6 | 2.60 | 1.3 | 2.4 | 2.60 | 1.8 | 1.6 | 3.2 | 3.89 |

[a] $n_1$ was obtained by integrating (cf. eq 1) from 0 to $r_1$ while $n_2$ was gotten by integrating from $r_1$ to $r_2$ ($r_i$ in Å). The coordination numbers are given by $n = n_1 + n_2$, where $n_1$ and $n_2$ correspond to the two peaks in $g_{1x}(r)$. Also shown is $n$ for $g_{1yz}(r)$.

**Special-Pair Dance.** We now show that the distortion of the Eigen cation is dynamic and characterize the distortion mode in detail. Figure 3 shows that, during the long non-transfer intervals (HCTH and MS-EVB3 trajectories), when the protonated oxygen maintains its identity (lower panels), that of $O_{1x}$ fluctuates between three values (upper panels), namely, the three water ligands in the first solvation shell of the $H_3O^+$. For the qMS-EVB3 and the MS-EVB2 simulations (Figure S1 in Supporting Information), for which PT events are much more frequent, there is less available time for $O_{1x}$ identity changes.

To probe this partner-switch statistically, we present in Figure 7A the average number of different 1$x$ partners as a function of time, whereas Figure 7B shows their average rate of exchange. These data depend surprisingly little on the water model (shown here are MS-EVB3, AIMD/HCTH, and qMS-EVB3 data). For very short segments, there is exactly one partner and a zero exchange rate. These segments are thus dominated by tight Zundel complexes. For long segments, there are exactly three different partners and an exchange rate of one per 40 fs (somewhat slower for quantal nuclear dynamics, qMS-EVB3). The triple-coordination is indicative of an Eigen complex in which the special partner varies dynamically. This "special pair dance" (SP-dance) rapidly randomizes the direction in which the proton eventually moves, making PT in water a random-walk, diffusive process,[6] rather than a coherent transfer over a range of water molecules as previously perceived.

It is also possible to identify the HB cleavage event that drives the SP-dance. The areas under the $O_{1x}$ and $O_{1yz}$ peaks in Figure 6 yield coordination numbers of $n = 3.1$ and $n = 3.7$, respectively. Because A1 bonds are markedly weaker than D1 bonds,[48] the missing HB to $O_{1x}$ is mostly an A1 bond. It follows that cleavage of an A1 HB to a $y$ oxygen could be a prerequisite for it to become the new special partner.

We test this in the time domain by monitoring the number of A1 bonds to oxygens $O_{1x}$ and $O_{1y}$ (first and second closest partners in the first solvation shell) before and after the partner exchange during long non-transfer intervals (>500 fs; see below), when the proton resides continuously on the same oxygen. This is shown in Figure 8, where $t = 0$ is the time of partner exchange. Results were then averaged over 10 ns of a room temperature MS-EVB3 trajectory. In agreement with the area under the equilibrium $g(r)$ discussed above, we find that the probability of having an A1 HB to $O_{1x}$ is only 0.1. This HB is essentially nonexistent, just like an acceptor HB to the

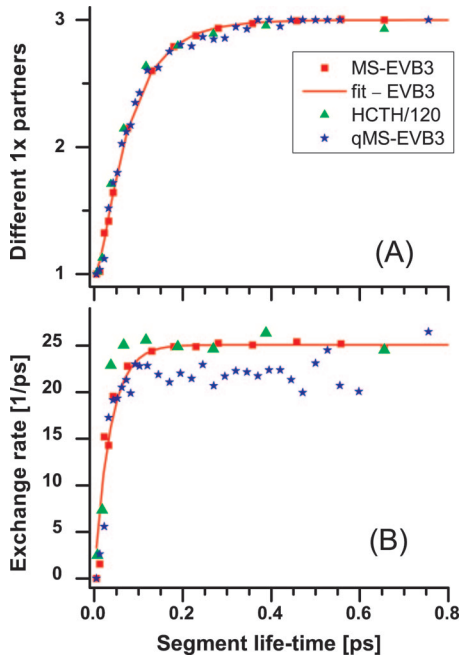


**Figure 7.** (A) Average number of different special partners, $O_{1x}$, as a function of the non-transfer interval length, $t$, for three simulation protocols (classical and quantal MS-EVB3 and DFT with the HCTH functional). Line is a fit of the MS-EVB3 data to $1 + 2[1 - \exp(-t/\tau_1)][1 - \exp(-t/\tau_2)]$ with $\tau_1 = 30$ fs and $\tau_2 = 80$ fs. (B) Average rate of exchanging the 1x partner, fitted to the function $a[1 - \exp(-t/\tau)]$ with $a = 25$ ps$^{-1}$ and $\tau = 36$ fs (MS-EVB3).

hydronium itself. The probability of having an A1 HB to $O_{1y}$ is 0.3−0.4, as compared with 0.7 for $O_{1yz}$ from the equilibrium $g(r)$. The role of the A1 bond in partner exchange kinetics is clearly discernible from the figure: On average, about 100 fs before the exchange, the HOH···$O_{1y}$ bond starts to break. Once both water molecules ($x$ and $y$) in the hydronium first-shell lose their A1 bonds, their distances to the central $H_3O^+$ modulate via an asymmetric HB stretching mode (not shown). During such periods, the $O_{1x}$ identity fluctuates between only two values (Figure 3). Subsequent to the exchange (i.e., for $t > 0$ in the figure), the probability of having an A1 bond to what has been $O_{1x}$ (and is now $O_{1y}$) increases rapidly. Thus, cleavage of an A1 bond is likely to be rate-limiting toward partner exchange whenever this bond exists.

The depiction of the SP-dance as a special-partner switch, which is triggered by A1 cleavage, is strikingly similar to the description of PT in water according to the first AIMD simulations.[20,21] It could be that these pioneering works identified the SP-dance as being actual PT, which rather occurs on a slower time scale.[37] The data presented there is insufficient for differentiating between the two possibilities. From the more detailed analysis presented here, it appears that the SP-dance is a pretransfer stage representing repeated trials to find a suitable PT partner.

**Conditional RDFs and the Transition Structure.** We shall now present additional evidence showing that the SP is not the same as the $H_5O_2^+$ transition complex. The latter has an even shorter central HB and it occurs only close to a PT event. To proceed, we consider conditional RDFs for the long and short trajectory segments discussed above. Ideally, these segments should be infinitely long or short, but practically the asymptotic behavior is approached for segments shorter than a few 10s of fs or longer than a few 100s of fs, respectively. One indication for the existence of the two limits was seen in Figure 7: Below 10 fs, there is a single partner which does not exchange, whereas

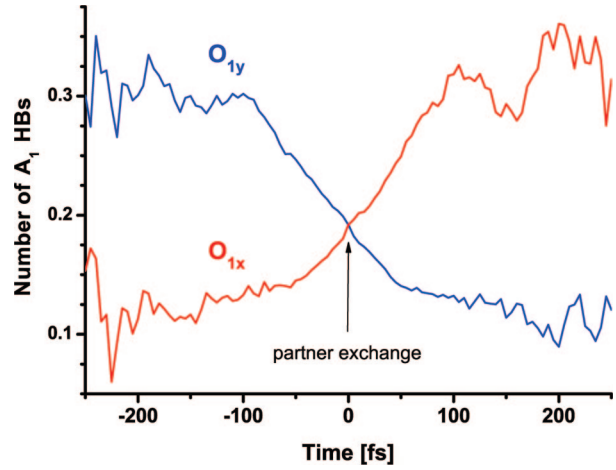


**Figure 8.** Average number of A1 HBs donated to oxygens $O_{1x}$ and $O_{1y}$ in the hydronium solvation shell. Time $t = 0$ is when these two oxygens switch their role as special partners to the hydronium. To eliminate contribution from Zundel structures, the average was performed over non-transfer intervals larger than 500 fs (within a 10 ns of room-temperature MS-EVB3 trajectory), after eliminating the first and last 50 fs from each segment.

for $t > 400$ fs there is a fixed number of partners (three), which exchange at a fixed rate. We wish to establish the structure of the hydrated proton in these two limits, showing that it corresponds to the Zundel and Eigen cations, respectively.

We thus define "conditional RDFs" as those averaged over the subensembles of "short" and "long" trajectory segments (non-transfer intervals). In the second case, we eliminate also the first and last 50 fs, where the configuration is close to a PT state. Figure S3 in Supporting Information shows that the conditional $g_0(r)$, restricted to these two subensembles, tend indeed to two limiting forms when $t \to 0$ or $t \to \infty$. It verifies our expectation that these limits are practically achieved for segments shorter than 10 fs and longer than 300 fs, respectively. Since we have sufficient statistics, we have defined the long segments here as $t > 500$ fs ($t > 400$ fs for AIMD, where less statistics is available).

Figure 9 (upper panels) shows that $g_0(r)$ is completely different for the two ensembles. In case (a), it is similar to the equilibrium $g_0(r)$ in Figure 6, except that it is narrower, higher, and misses the short-distance shoulder. We attribute this to the Eigen cation, which is thus the "resting state" of the proton. In case (b), there is a double peak, with the left peak down-shifted by nearly 0.1 Å as compared with the corresponding peak of the equilibrium $g_{1x}(r)$ RDF in Figure 6. We attribute this $g_0(r)$ to the Zundel cation.

Figure 9 also shows how the equilibrium $g_0(r)$ (in black) can be decomposed into a linear combination of the two basic RDFs

$$g_0^{Equil.}(r) = f g_0^{Long}(r) + (1 - f) g_0^{Short}(r) \qquad (2)$$

The adjustable parameter $f$ is the fraction of the Eigen state, which dominates the long segments. Using a least-squares criterion, we obtain the orange curves with the best-fit $f$ value of 0.72 for MS-EVB3. This corresponds to a Helmholtz (i.e., constant volume) free energy bias,

$$\Delta F = -RT \ln[f/(1 - f)] \qquad (3)$$

of −2.4 kJ/mol in favor of the Eigen cation at $T = 300$ K. The error in $\Delta F$ is sensitive to that in $f$: an error of, say, only 5% in $f$ translates to nearly 20% error in $\Delta F$. Alternative approaches for determining this free energy difference gave ≈−3.5 kJ/mol for the MS-EVB3 potential[37] and −2.5 kJ/mol for a classical

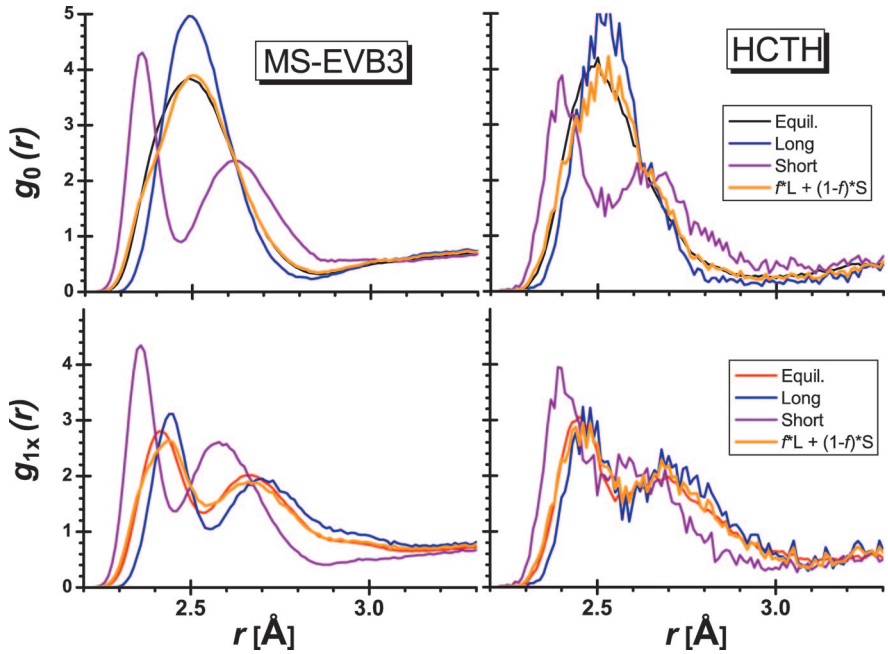


**Figure 9.** Conditional RDFs, $g_0(r)$ and $g_{1x}(r)$, for (a) long segments (blue), (b) short segments (purple), (c) all segments (black/red), and (d) a linear combination of (a) and (b) according to eq 2 (orange). $f = 0.72$ and 0.70 for MS-EVB3 and HCTH, respectively. Occupation numbers under the first two peaks, $n_1$ and $n_2$, are collected in Tables 2 and 3. See Figures S4 and S5 in Supporting Information for similar results for the other simulation models.

AIMD/BLYP calculation.[41] The description established herein, of protonated water as a "mixture" of Eigen and Zundel cations, should be understood in a statistical sense. The ensemble is not composed of a mixture of two discrete conformations but rather of a plethora of geometries. It is only their RDF—a statistical distribution—which is decomposed into a linear combination of RDFs characterizing the two components.

Our analysis is corroborated by a similar decomposition for $g_{1x}(r)$, shown in Figure 9 (bottom panels). We also note that for the short segments (purple lines) $g_{1x}(r)$ is quite similar to $g_0(r)$, particularly their first identical peak at 2.36 Å (MS-EVB3), which is due to the $O_0-O_{1x}$ HB. This short internuclear distance indicates that the dominant protonated water structure during the short trajectory segments is $H_5O_2^+$. The fact that the secondary peaks do not precisely coincide suggests that the $O_0-O_{1y}$ and $O_{1x}-O_{2x}$ distances are different, so that the transition structure is a distorted Zundel complex. For the long segments, $g_{1x}(r)$ (blue line) is similar to the equilibrium one (Figure 6), only slightly shifted to longer distances. This $g_{1x}(r)$ depicts more precisely (than the equilibrium one) the SP which exists during long PT-free time intervals. Its structure is thus clearly distinguishable from the distorted Zundel complex (purple line) which exists close to the transition.

This procedure works successfully for the other classical methodologies (Figures S4 and S5 of Supporting Information) but less so for the qMS-EVB3 trajectory, suggesting that quantal effects make the distinction between the two conformations fuzzy, as previously suggested.[23,32,33] Then it becomes difficult to represent the equilibrium RDF as a linear combination of RDFs for the two limiting structures.

It is interesting to compare our procedure for obtaining the Eigen and Zundel $g_0(r)$, based on the temporal distance from the transition structure, to the procedure which is based on a geometric criterion.[23,41] Here, one monitors the distance, $\delta$, of the proton in the special bond, $O_0\cdots H^+\cdots O_{1x}$, from its midpoint. All of the configurations where $|\delta| < \Delta_Z$ are branded as Zundel complexes, whereas all of those with $|\delta| > \Delta_E$ are considered Eigen complexes, where they chose $\Delta_Z$ and $\Delta_E$ as 0.1 and 0.3 Å, respectively. This choice was apparently motivated by the thought that 0.1 Å is sufficiently close to zero whereas 0.3 Å is the minimum of a free energy curve (e.g., Figure 2 in ref 41). In Figure S6 of Supporting Information, we have calculated the two $g_0(r)$ for various choices of the $\Delta$'s. There is a strong dependence of the RDF on the choice of this parameter. For a Zundel cation, $\Delta_Z = 0.1$ Å is indeed a good compromise between the requirement that $\Delta_Z \to 0$ and the need to generate statistics. However, for an Eigen cation, a comparison with our conditional RDF for long intervals shows that $\Delta_E$ should better be reduced to 0.2 Å (Figure S6). The configurations sampled now are on both sides of the minimum in the Helmholtz free energy.

Figure 10 compares the two RDFs, with the optimal $\Delta$'s, to our conditional RDFs obtained for the short and long intervals. The (qualitatively) good agreement between the two measures clearly indicates that the structures close to the transition-state (short intervals) are Zundel structures (in terms of having the proton midway between the two oxygens), whereas those far from the transition state for PT are Eigen configurations. [Parenthetically we note that the Zundel $g_0(r)$ that we calculate from the criterion of Marx et al.[41] does not look like the dashed green line in their Figure 1a, which was apparently misplaced. Nevertheless, the Zundel-Eigen free energy difference in their Figure 2 is very similar to ours].

The geometric and energetic criteria investigated in this section point quite conclusively to the Eigen cation as the "resting state" of protonated water and the Zundel cation as a transition-state for PT. The latter exists only near PT events and is several kilojoules per mole higher in energy than the Eigen cation. These qualitative results appear to be independent of both the water model (MS-EVB vs AIMD potentials) and the nature of the nuclear dynamics (classical vs quantal). Thus, we conclude that the ZZ mechanism,[5,30,42] with a more stable Zundel cation, is improbable. Proton mobility in water appears

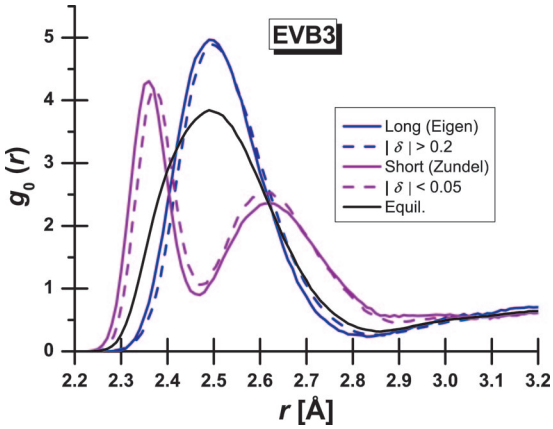


**Figure 10.** Comparison of the conditional RDFs for Short and Long non-PT intervals, Figure 9 (full lines), with the geometric definition of Marx et al.[41] (dashed lines) using $\Delta_Z = 0.05$ and $\Delta_E = 0.2$ Å (see text for details). Figure S6 in the Supporting Information was used to determine these "best values" for these two parameters.

to proceed exclusively through the EZE transition, in agreement with the prediction made in 1995.[15,16]

**Time-dependent RDFs Capture the PT Event.** We now proceed to capture the protonic transition in real time. To do so, we consider all PT events that have the $H_3O^+$ localized on the same oxygen atom for at least 50 fs prior to the proton hop. The choice of 50 fs long intervals is a compromise between the need to start sufficiently far from the transition state and the need to generate sufficient statistics (the probability of long non-transfer intervals diminishes exponentially; see Figure 4). A comparison with the conditional Eigen RDF of Figure 9 will allow us to establish (below) that 50 fs before the transition the average conformation of protonated water is already sufficiently close to the Eigen structure.

Choosing the PT event as the zero of time, $t = 0$, we average the RDFs $g_0(r)$ and $g_{1x}(r)$ for each respective time frame before (and after) PT over the whole above-mentioned trajectory segment ensemble. As a result, we obtain the time-dependent RDF (TD-RDF), $g_0(r; t)$ and $g_{1x}(r; t)$. These provide a "movie" that shows, on the average, how the water structure around the hydronium develops near a proton hop. By synchronizing $t = 0$ for all TD-RDFs to be the PT event, we thus generate statistically meaningful RDFs for kinetic rather than thermodynamic properties of the liquid state.

Figures 11 and 12 show such a time evolution for MS-EVB3 and qMS-EVB3 trajectories. Already 40 fs before the transition, the hydronium structure is that of the Eigen ion. This follows because $g_0(r;-40)$ and $g_{1x}(r;-40)$ coincide with $g_0(r)$ and $g_{1x}(r)$, respectively, as obtained from the long trajectory segments (Figure 9). As the transition is approached, the first peak of both RDFs moves inward, to shorter distances, until at PT they coalesce and coincide with the first peak of the Zundel RDF as determined above from the short trajectory segments (Figure 9). During this propagation, the peak in $g_0(r; t)$ splits, developing the double-peak structure characteristic of the $H_5O_2^+$ ion. This gives a vivid demonstration for the EZE transition as driving PT in protonated liquid water.[15]

In contrast, the second peak of $g_{1x}(r;t)$ changes relatively little. Thus, the distance between $O_{1x}$ and $O_{2x}$ (Figure 2) remains almost constant during the transition. This suggests that the $(H_2O)_2H_3O^+$ moiety composed of the hydronium with its two $O_{1yz}$ ligands is moving toward a nearly static $O_{1x}$ as the Zundel complex is formed. It appears then that the HBs on the $yz$ side weaken considerably before PT. This is supported by the

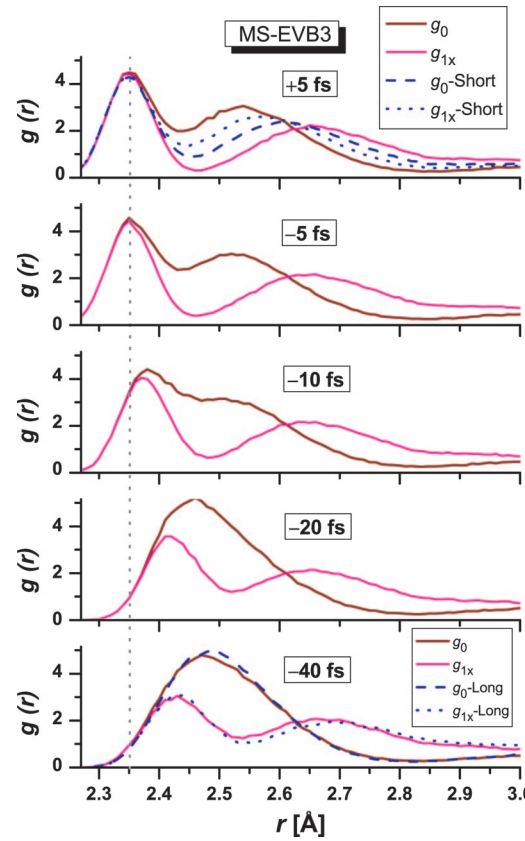


**Figure 11.** Time dependent RDFs for the MS-EVB3 water model, $g_0(r; t)$, brown, and $g_{1x}(r; t)$, magenta, reveal the average water structure surrounding the hydronium immediately before and after the PT event. The RDFs in the first and last time frames are compared with the conditional RDFs of Figure 9 (dashed/dotted blue lines).

observation that in the quantum trajectory (qMS-EVB3) the second peak in $g_0(r; t)$, which arises from the $O_0-O_{1yz}$ bonds, is smeared out (Figure 12) suggesting that these bonds become energized near the transition.

## Conclusions

The mechanism of proton mobility in liquid water occurs on a hierarchy of time and distance scales. This makes its elucidation a challenge. We have used five different water models and simulation techniques to probe this mechanism. Although actual PT rates differ by factors of 2 to 3 between simulation methods and potential functions, the qualitative details of the mechanism depend only weakly on them. Rather, establishment of the mechanism requires appropriate statistical approaches with sufficiently large ensembles of time frames that allow one to draw meaningful conclusions.

Our statistical analysis probed predominantly the processes occurring during the non-transfer time intervals, up to the first PT event (regardless of whether it is fruitful or recurrent). We have introduced conditional and time-dependent RDFs which demonstrate that the equilibrium structure of protonated water dominant away from the transfer event is an Eigen cation, $H_3O^+[3H_2O]$,[14] whereas the Zundel cation, $H_5O_2^+$, occurs with observable statistical weight only as a transition structure close to PT events. Interestingly, this has now been verified by photoelectron spectroscopy,[46,47] lending further support to the EZE scenario.[15]

Nevertheless, the Eigen complex is not symmetric:[32] One HB (to the $O_{1x}$ ligand) is consistently shorter than the other two,

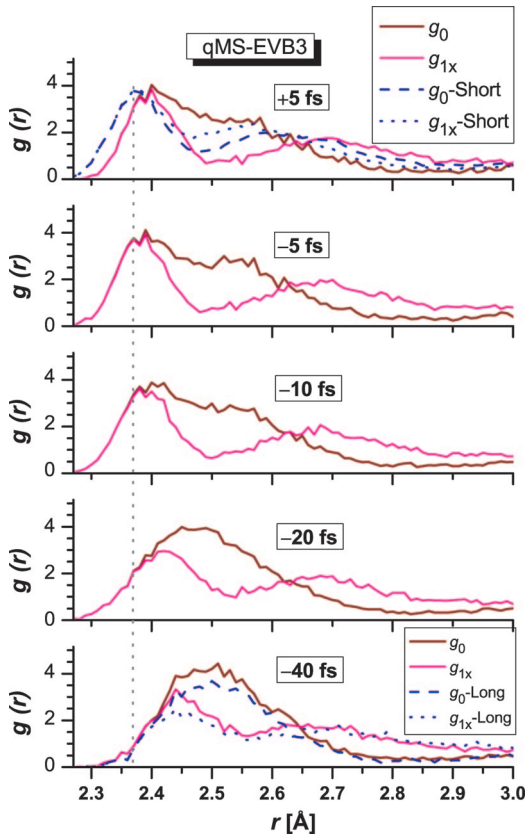


**Figure 12.** Same as Figure 11 for a quantal MS-EVB3 trajectory. See Figures S7−S9 in Supporting Information for the other water models.

forming a SP,[20,21] whereas another HB is longer than average.[42] This widens the first peak in the RDF but not sufficiently to split it into a double peak, as expected for the Zundel cation. The latter is a more severe distortion of the SP which occurs predominantly close to a PT event.

The distorted Eigen cation is not static. Rather, its closest ($O_{1x}$) ligand constantly changes its identity within the first solvation-shell. This "SP-dance", depicted schematically in Figure 13, represents repeated trials to locate a suitable partner for the PT act. Before the exchange, the probability of having an A1 HB to $O_{1y}$ diminishes, whereas after the exchange it increases (Figure 8). This resembles the description of PT events in the early AIMD reports,[20,21] except that partner exchange takes place, on the average, every 40 fs, whereas it takes several picoseconds for a PT to occur. Consequently, we observe in Figure 3 several special-pair switches between the three first-shell ligands during the long segments of a "resting" hydronium.

Participation of A1 cleavage in the faster partner exchange events (rather than in the slower PT) is in line with previous calculations showing that A1 HBs are much weaker than typical water−water HBs,[48] apparently due to the unfavorable interaction of a water hydrogen with the positive center. For this reason, the frequency of partner switches depends more weakly on temperature than PT, so we expect the importance of the SP-dance to diminish at higher temperatures (we have verified this qualitatively for the qMS-EVB3 potential). Likewise, simulations with faster PT (such as the MS-EVB2 and qMS-EVB3) exhibit less of an SP-dance.

The outcome of the SP-dance is equivalent to diffusional rotation of the $H_3O^+$, as suggested by Hückel,[12] except that no rotational motion is involved. This phenomenon rapidly randomizes the proton hop direction, so that proton mobility in water is diffusive rather than coherent (i.e., it does not involve correlated hopping over long HB water chains as previously anticipated).[14] Indeed, time-resolved fluorescence measurements from molecules exhibiting excited-state PT to

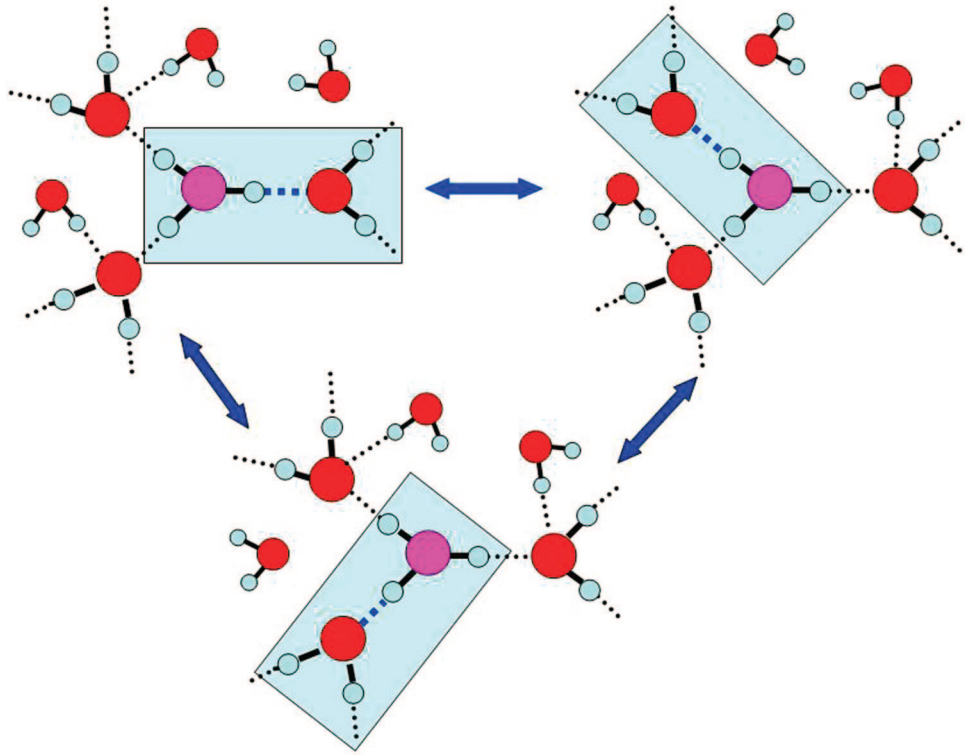

**Figure 13.** Schematic depiction of the "special pair dance" occurring in the first solvation-shell of the hydronium in its "resting state" (during the long trajectory segments of no-PT). Oxygens in red, except for the hydronium oxygen in magenta.

water can be explained by a diffusive proton as of about 20 ps after its dissociation.[6,63] However, this may change when a proton hops between donor and acceptor that, according to recent time-resolved IR measurements, may induce intervening water molecules to form proton wires of up to 5 units long.[64–67] This effect is outside the scope of the present work.

The PT step in the Grotthuss mechanism begins when the hydronium "selects" one of the dancing partners by moving, together with its 1*y* or 1*z* ligands, an additional distance (of nearly 0.1 Å) in its direction. This forms the transition complex, a distorted Zundel $H_5O_2^+$ ion, as shown schematically in Figure 14. Now, primarily, the hydronium moves and not $O_{1x}$, because the second peak of $g_{1x}(r)$ remains nearly time invariant during the transition (Figure 11), suggesting a constant $O_{1x}-O_{2x}$ distance.

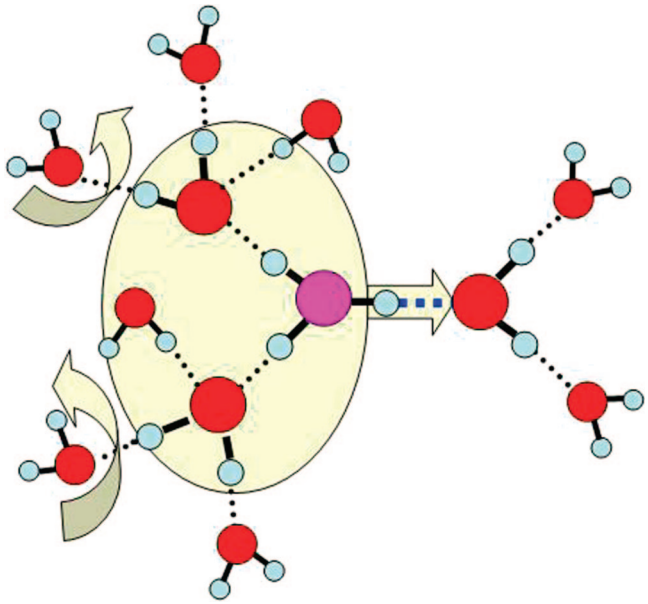

**Figure 14.** Schematic depiction of the "selection phase" leading into the transitional Zundel structure of the proton mobility mechanism. Simultaneous cleavage of several D1 HBs on the *yz* side allows the hydronium with its first-shell *yz* ligands to move in the *x* direction toward $O_{1x}$ and form a Zundel complex. Straight arrow denotes translation, whereas curly arrows denote (the suggested)[36] cleavage of a HB, probably by a combination of translation and rotation.

The selection step ends the epoch during which the proton resides continuously on a single oxygen. The statistics of such time intervals is multiexponential, as shown in Figure 4. Now a transition Zundel structure is formed, in which the proton may rattle many times between the two oxygens before eventually a new Eigen complex forms. Thus, PT is truly a hierarchical process, involving partner exchange, partner selection, rattling, and eventually settling into the new Eigen configuration.

What then enables PT to occur? The cleavage of an A1 HB to $O_{1x}$ as a rate-limiting step (Figure 1)[3,15,23] was shown to correlate with the faster partner exchange, rather than the slower PT events. Commensurate with this observation, we find that $O_{1x}$ has, on average, $n = 3.1$ partners, namely, only 0.1 of an A1 HB. Its A1 bond was lost already during the SP dance, before the selection step took place.

It appears, therefore, that the activation enthalpy for proton mobility is concealed in the selection step which allows the distorted Zundel intermediate to form. This step apparently consists of hydronium translation. Because the $H_3O^+$ is bound to its first-shell ligands by superstrong HBs (D0),[17,48] it likely moves in concert with its $O_{1yz}$ ligands. To allow such motion, some of the D1 HBs to $O_{1y}$ and/or $O_{1z}$ might have broken (curved arrows in Figure 14). Here, we have considered only A1 HB cleavage events correlating with partner exchange in the SP-dance but not on D1 cleavage during the PT step itself. Nevertheless, the latter is in agreement with the suggestion by Lapid et al.[36] that several D1 bonds break on the *yz* side, making proton mobility a truly cooperative phenomenon.

**Acknowledgment.** This research was supported in part by the United States-Israel Binational Science Foundation (BSF) Grant 2006067 (N.A. and G.A.V.) and the United States National Science Foundation Grant CHE-0719522 (G.A.V.). The Fritz Haber Center is supported by the Minerva Gesellschaft für die Forschung, München, FRG.

**Supporting Information Available:** Special pair dance movie and supporting figures. This material is available free of charge via the Internet at http://pubs.acs.org.

## References and Notes

(1) Swanson, J. M. J.; Maupin, C. M.; Chen, H.; Petersen, M. K.; Xu, J.; Wu, Y.; Voth, G. A. *J. Phys. Chem. B* **2007**, *111*, 4300.
(2) Voth, G. A. *Acc. Chem. Res.* **2006**, *39*, 143.
(3) Marx, D. *ChemPhysChem* **2006**, *7*, 1848. Addendum: ibid. *8*, 209.
(4) Wraight, C. A. *Biochim. Biophys. Acta* **2006**, *1757*, 886.
(5) Kreuer, K.-D.; Paddison, S. J.; Spohr, E.; Schuster, M. *Chem. Rev.* **2004**, *104*, 4637.
(6) Agmon, N. *J. Phys. Chem. A* **2005**, *109*, 13.
(7) de Grotthuss, C. J. T. *Ann. Chim.* **1806**, *LVIII*, 54.
(8) Cukierman, S. *Biochim. Biophys. Acta* **2006**, *1757*, 876.
(9) Danneel, H. Z. *Elektrochem.* **1905**, *11*, 249.
(10) Latimer, W. M.; Rodebush, W. H. *J. Am. Chem. Soc.* **1920**, *42*, 1419.
(11) Huggins, M. L. *J. Phys. Chem.* **1936**, *40*, 723.
(12) Hückel, E. Z. *Electrochem.* **1928**, *34*, 546.
(13) Bernal, J. D.; Fowler, R. H. *J. Chem. Phys.* **1933**, *1*, 515.
(14) Eigen, M. *Angew. Chem., Int. Ed.* **1964**, *3*, 1.
(15) Agmon, N. *Chem. Phys. Lett.* **1995**, *244*, 456.
(16) Agmon, N.; Goldberg, S. Y.; Huppert, D. *J. Mol. Liquids* **1995**, *64*, 161.
(17) Agmon, N. *J. Chim. Phys. Phys.-Chim. Biol.* **1996**, *93*, 1714.
(18) Agmon, N. *Israel J. Chem.* **1999**, *39*, 493.
(19) Zundel, G. *The Hydrogen Bond, Recent Developments in Theory and Experiments*; Schuster, P., Zundel, G., Sandorfy, C., Eds.; North Holland: Amsterdam, 1976; pp 687−766.
(20) Tuckerman, M.; Laasonen, K.; Sprik, M.; Parrinello, M. *J. Phys. Chem.* **1995**, *99*, 5749.
(21) Tuckerman, M.; Laasonen, K.; Sprik, M.; Parrinello, M. *J. Chem. Phys.* **1995**, *103*, 150.
(22) Tuckerman, M. E.; Marx, D.; Klein, M. L.; Parrinello, M. *Science* **1997**, *275*, 817.
(23) Marx, D.; Tuckerman, M. E.; Hutter, J.; Parrinello, M. *Nature* **1999**, *397*, 601.
(24) Lobaugh, J.; Voth, G. A. *J. Chem. Phys.* **1996**, *104*, 2056.
(25) Schmidt, R. G.; Brickmann, J. *Ber. Bunsen-Ges. Phys. Chem.* **1997**, *101*, 1816.
(26) Zahn, D.; Brickmann, J. *Israel J. Chem.* **1999**, *39*, 469.
(27) Vuilleumier, R.; Borgis, D. *J. Mol. Struct.* **1997**, *436−437*, 555.
(28) Vuilleumier, R.; Borgis, D. *J. Phys. Chem. B* **1998**, *102*, 4261.
(29) Vuilleumier, R.; Borgis, D. *J. Chem. Phys.* **1999**, *111*, 4251.
(30) Vuilleumier, R.; Borgis, D. *Israel J. Chem.* **1999**, *39*, 457.
(31) Schmitt, U. W.; Voth, G. A. *J. Phys. Chem. B* **1998**, *102*, 5547.
(32) Schmitt, U. W.; Voth, G. A. *J. Chem. Phys.* **1999**, *111*, 9361.
(33) Schmitt, U. W.; Voth, G. A. *Israel J. Chem.* **1999**, *39*, 483.
(34) Day, T. J. F.; Schmitt, U. W.; Voth, G. A. *J. Am. Chem. Soc.* **2000**, *122*, 12027.
(35) Day, T. J. F.; Soudackov, A. V.; Čuma, M.; Schmitt, U. W.; Voth, G. A. *J. Chem. Phys.* **2002**, *117*, 5839.
(36) Lapid, H.; Agmon, N.; Petersen, M. K.; Voth, G. A. *J. Chem. Phys.* **2005**, *122*, 014506.
(37) Wu, Y.; Chen, H.; Wang, F.; Paesani, F.; Voth, G. A. *J. Phys. Chem. B* **2008**, *112*, 467.
(38) Lill, M. A.; Helms, V. *J. Chem. Phys.* **2001**, *115*, 7993.

(39) Car, R.; Parrinello, M. *Phys. Rev. Lett.* **1985**, *55*, 2471.
(40) Warshel, A.; Weiss, R. M. *J. Am. Chem. Soc.* **1980**, *102*, 6218.
(41) Marx, D.; Tuckerman, M. E.; Parrinello, M. *J. Phys.: Condens. Matter* **2000**, *12*, A153.
(42) Asthagiri, D.; Pratt, L. R.; Kress, J. D. *Proc. Natl. Acad. Sci., U.S.A.* **2005**, *102*, 6704.
(43) Kornyshev, A. A.; Kuznetsov, A. M.; Spohr, E.; Ulstrup, J. *J. Phys. Chem. B* **2003**, *107*, 3351.
(44) Woutersen, S.; Bakker, H. J. *Phys. Rev. Lett.* **2006**, *96*, 138305.
(45) Amir, W.; Gallot, G.; Hache, F.; Bratos, S.; Leicknam, J.-C.; Vuilleumier, R. *J. Chem. Phys.* **2007**, *126*, 034511.
(46) Winter, B.; Faubel, M.; Hertel, I. V.; Pettenkofer, C.; Bradforth, S. E.; Jagoda-Cwiklik, B.; Cwiklik, L.; Jungwirth, P. *J. Am. Chem. Soc.* **2006**, *128*, 3864.
(47) Kirchner, B. *ChemPhysChem* **2007**, *8*, 41.
(48) Markovitch, O.; Agmon, N. *J. Phys. Chem. A* **2007**, *111*, 2253.
(49) Levine, R. D. *Molecular Reaction Dynamics*; Cambridge University Press: New York, 2005.
(50) Izvekov, S.; Voth, G. A. *J. Chem. Phys.* **2005**, *123*, 044505. Erratum: ibid. **2006**, *124*, 039901.
(51) VandeVondele, J.; Mohamed, F.; Krack, M.; Hutter, J.; Sprik, M.; Parrinello, M. *J. Chem. Phys.* **2005**, *122*, 014515.
(52) Voth, G. A. *Adv. Chem. Phys.* **1996**, *93*, 135.
(53) Boese, A. D.; Doltsinis, N. L.; Handy, N. C.; Sprik, M. *J. Chem. Phys.* **2000**, *112*, 1670.
(54) CPMD V3.11 Copyright IBM Corp 1990−2006, Copyright MPI fuer Festkoerperforschung Stuttgart 1997−2001.
(55) Troullier, N.; Martins, J. L. *Phys. Rev. B* **1991**, *43*, 1993.
(56) Schwegler, E.; Grossman, J. C.; Gygi, F.; Galli, G. *J. Chem. Phys.* **2004**, *121*, 5400.
(57) Grossman, J. C.; Schwegler, E.; Draeger, E. W.; Gygi, F.; Galli, G. *J. Chem. Phys.* **2004**, *120*, 300.
(58) Chandra, A.; Tuckerman, M. E.; Marx, D. *Phys. Rev. Lett.* **2007**, *99*, 145901.
(59) Luzar, A.; Chandler, D. *Nature* **1996**, *379*, 55.
(60) Starr, F. W.; Nielsen, J. K.; Stanley, H. E. *Phys. Rev. E* **2000**, *62*, 579.
(61) Egelstaff, P. A. *An Introduction to the Liquid State*; Oxford University Press: Oxford, 2nd edition, 1994.
(62) Botti, A.; Bruni, F.; Ricci, M. A.; Soper, A. K. *J. Chem. Phys.* **2006**, *125*, 014508.
(63) Pines, E.; Huppert, D.; Agmon, N. *J. Chem. Phys.* **1988**, *88*, 5620.
(64) Mohammed, O. F.; Pines, D.; Nibbering, E. T. J.; Pines, E. *Angew. Chem., Int. Ed.* **2007**, *46*, 1458.
(65) Mohammed, O. F.; Pines, D.; Pines, E.; Nibbering, E. T. *J. Chem. Phys.* **2007**, *341*, 240.
(66) Siwick, B. J.; Bakker, H. J. *J. Am. Chem. Soc.* **2007**, *129*, 13412.
(67) Siwick, B. J.; Cox, M. J.; Bakker, H. J. *Biophys. J.* **2008**, *93*, 1571.

JP804018Y